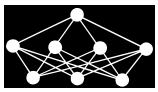

PREDICTION OF SLOPE STABILITY BASED ON GA-BP HYBRID ALGORITHM

Xinhua Xue[*], *Yangpeng Li*[*], *Xingguo Yang*[*], *Xin Chen*[*], *Jian Xiang*[†]

Abstract: Safety monitoring and stability analysis of high slopes are important for high dam construction in mountainous regions or precipitous gorges. Slope stability estimation is an engineering problem that involves several parameters. To address these problems, a hybrid model based on the combination of Genetic algorithm (GA) and Back-propagation Artificial Neural Network (BP-ANN) is proposed in this study to improve the forecasting performance. GA was employed in selecting the best BP-ANN parameters to enhance the forecasting accuracy. Several important parameters, including the slope geological conditions, location of instruments, space and time conditions before and after measuring, were used as the input parameters, while the slope displacement was the output parameter. The results shown that the GA-BP model is a powerful computational tool that can be used to predict the slope stability.

Key words: *GA-BP hybrid algorithm, Jinping I hydropower station, left abutment slope, stability*

Received: February 24, 2014 **DOI:** 10.14311/NNW.2015.25.010
Revised and accepted: April 13, 2015

1. Introduction

The accurate estimation of the stability of a rock or soil slope is a difficult problem mainly because of the complexity of the physical system itself and the difficulty involved in determining the necessary input data associated with geotechnical parameters [8]. The methods most commonly used at present for slope stability analysis are the rigid-body limit equilibrium method and the finite element method (FEM) [6]. The former yields a safety factor determined by analyzing the limit equilibrium status of a block. The method is characterized by clear concepts and simple calculations. However, it cannot take nonlinear structural deformation into account, and the method assumes that sliding surfaces reach an ultimate state of failure simultaneously, which does not reflect the actual stress status of slip surfaces

[*]Xinhua Xue – Corresponding Author, Yangpeng Li, Xingguo Yang, Xin Chen, State Key Laboratory of Hydraulics and Mountain River Engineering, College of Water Resource and Hydropower, Sichuan University, Chengdu, Sichuan, 610065, P.R.China. E-mail: scuxxh@163.com, 306106438@qq.com, 89022251@163.com, 1013400585@qq.com, Tel: +86 13708026185, +86 13684045807, +86 2885465055, +86 2885463828

[†]Jian Xiang, Sinohydro Bureau 7 Co., Ltd., Chengdu, Sichuan, 610081, P.R.China. E-mail: xiangjianqj@163.com, Tel: +86 13980987962

[9]. FEM can be used to determine the stress field and displacement field of the slope but cannot yield a specific value for the slope stability safety factor. Although many researchers have obtained slope stability safety factors using the strength reduction method together with finite element analysis [2, 3], this method requires certain failure criteria by which to judge whether a system enters a limit equilibrium state. Therefore, the estimation of slope stability using the conventional methods is not an easy task and it requires sophisticated modeling techniques, experience, deep knowledge of engineering and a vast amount of experimental data.

In recent years, there have been several attempts to use intelligent computational systems such as Artificial Neural Network in geotechnical engineering. This growing interest among researchers is stemming from the fact that these learning machines have an excellent performance in the issues of pattern recognition and the modeling of non-linear relationships of multivariate dynamic systems. In particular, several researchers had investigated the use of ANN in predicting the stability of slopes and their behavior under different types of loading. As a result, several successful applications of ANN that investigated slope stability and evaluated slope failure characteristics have been conducted [1, 7]. Although this is successful in many regards, ANN has also several inherent drawbacks such as over fitting, slow convergence, poor generalizing performance, and arriving at local minimum, and so on. These inherent limitations wherein the information or the intervening steps are not available have made ANN have the reputation of being a "black box" approach [4]. Therefore, alternative methods are needed, which can predict the slope stability more accurately.

This paper investigates the potential of GA-BP model for prediction of slope stability. GA was employed in selecting the best BP-ANN parameters to enhance the forecasting accuracy. Several important parameters, including the slope geological conditions, location of instruments, space and time conditions before and after measuring, were used as the input parameters, while the slope displacement was the output parameter. Then, the left abutment slope of Jinping I hydropower station serves as an example to check the GA-BP model's validity. The results shown that the GA-BP model is a powerful computational tool that can be used to predict the slope stability.

2. Engineering background

Jinping I hydropower station is located at the sharp bend of Jinping on the middle reach of Yalongjiang River, near Xichang (27°32′–28°10′ N, 101°46′–102°25′ E), about 500 km southwest of Chengdu, Sichuan province, PR China. It is situated within the slope transition zone from the Qinhai-Tibet Plateau to the Sichuan Basin. The project consists of a concrete double-curvature arch dam, diversion tunnels on the right bank, flood discharge and energy dissipation structures. The arch dam is 305 m in height, the highest one under construction in the world. The total reservoir capacity is 7.76×10^9 m^3 at a normal water level of 1880 m and the annual regulating reservoir capacity is 4.91×10^9 m^3 [10].

The dam site is located in the region composed of precipitous gorges and a sharply incised valley. Relative height difference of slopes can reach up to 1000–1700 m, with a declination of 30°–90°. The entire right bank and two thirds of the

downstream left bank are hosted on rock group $T^2_{2\text{-}3Z}$, which predominantly consists of marble with schist interbeds. Above the elevations of 1820–1900 m, the rocks in the left bank mainly consist of metasandstone and slate of group $T^3_{2\text{-}3Z}$. Complex geological structure, together with variable strata and stress-relief disturbance, has affected the stability of rock masses on both sides of the river. The left bank slope, with ridges and gutters around, is cut by bedding planes that have a stride towards the hillside, with inclinations of 55°–70°.

The total height of excavated slope on the left abutment is approximately 530 m, and the maximum horizontal excavation depth is 130 m. The maximum excavation width is 350 m, and the total excavation volume reaches 5.50×10^6 m^3. As far as concerned, the left abutment slope is one of the hydropower projects with the largest excavation scale in rock engineering. The geological condition is considerably complex and the stability situation is not encouraging, as shown in Figs. 1–2.

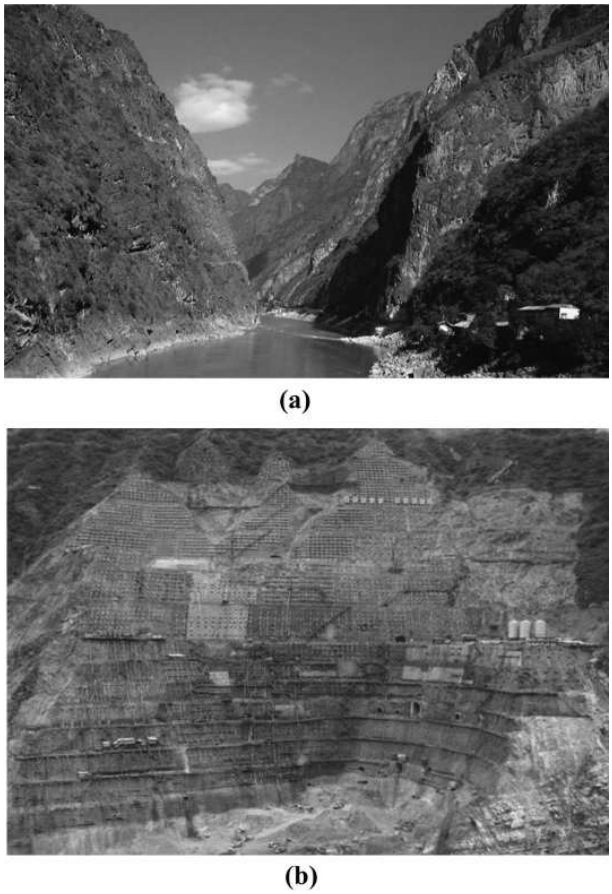

Fig. 1 *Geomorphic photograph of dam site: (a) before excavation, and (b) the left slope after excavation [13].*

Fig. 2 *Zone of crushed weak rock in the left dam abutment of Jinping I [12].*

3. GA-BP hybrid algorithm

Genetic algorithm (GA) is a search algorithm based upon the mechanics of natural selection, derived from the theory of natural evolution [5]. GA simulates mechanisms of population genetics and natural rules of survival in pursuit of the ideas of adaptation. A GA starts with a population of chromosomes, which are combined through genetic operators to produce successively fitter chromosomes. The genetic operators used in the reproductive process are selection, crossover, and mutation. In this work, the initial weights and thresholds of BP neural network were optimized by using the global-searching characteristic of GA, so that the forecast property is optimized effectively, the forecast precision and the generalization ability of the model are improved, and the convergence rate is raised. The main procedure of the GA-BP method is illustrated as follows:

(1) Selection of sample parameters and data normalization

Because the factors that affect the forecast results are of large numbers and very complex, it is important to select the input parameters correctly. The parameters that are closely related to the forecast results should be selected and they should be minimized as far as possible when the precision demand is met.

As each kind of the collected data has inconsistent unit, to speed up the convergence of the network training and meeting the output requirements of the network at the same time, all of the primary data should be normalized within $[-1, 1]$ before training the improved BP neural network model.

(2) Encoding and Initialization

Various encoding methods have been created for particular problems to provide effective implementation of genetic algorithms. There are mainly two ways to encode the connection weights and thresholds in the ANNs. One is

binary encoding; the other is real number encoding. Binary encoding is the most common one, mainly because the first research of GA used this type of encoding and because of its relative simplicity. In binary encoding, every chromosome is a string of bits 0 or 1. In spite of all that, binary encoding for function optimization problems is known to severe drawbacks due to the existence of Hamming cliffs, pairs of encoding having a large Hamming distance (the Hamming distance between two bit strings is defined as the number of corresponding positions in these bit strings where the bits have a different value) while belonging to points of minimal distance in phenotype space. To cross the Hamming cliff, all bits have to be changed simultaneously. The probability that crossover and mutation will occur can be very small. In this sense, the binary code does not preserve the locality of points in the phenotype space. Real number encoding is best used for function optimization problems. It has been widely confirmed that real number encoding perform better than binary encoding for function optimization and constrained optimizations problems. In real number encoding, the structure of genotype space is identical to that of the phenotype. Therefore, it is employed to encode the weights and thresholds of the BP neural network (also shown in Fig. 3) in this study.

As can be seen from Fig. 3, the structure of the BP neural network consists of an input layer, hidden layer and output layer. Suppose I and O represent the input and output dimensions, respectively. S stands for the hidden layer nodes, $\mathbf{W}_1$ for the connection weight matrix from the input layer to the hidden layer and $\mathbf{W}_2$ for the connection weight matrix from the hidden layer to the output layer. The first part of coding is $\mathbf{W}_1$, followed by $\mathbf{W}_2$, then following the threshold values $\mathbf{B}_1$, $\mathbf{B}_2$. Therefore, the length of chromosome should be $L = I \times S + S \times O + S + O$, namely, a chromosome is constituted by genes with the number of L, as shown in Fig. 4. After coding the weights and thresholds of the BP neural network, chromosome is generated at random and makes up an initial population.

(3) Calculation of fitness values

The individual fitness value is formulated as

$$f_i = 2 \Big/ \sum_{t=1}^{N} (y_t - \bar{y}_t)^2, \tag{1}$$

where f_i the fitness value of individual i, y_t the network output value, $\bar{y}_t$ the expected output value, and N is the number of output nodes. According to a certain proportion, the individuals of the highest fitness are selected, and directly entailed to the next generation.

(4) Genetic operators

Selection: The selection probability P_i is formulated as

$$P_i = f_i \Big/ \sum_{k=1}^{M} f_k, \tag{2}$$

where M is the population size.

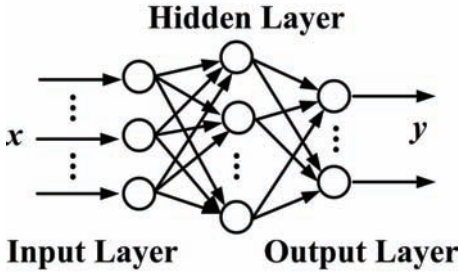

Fig. 3 *BP neural network model.*

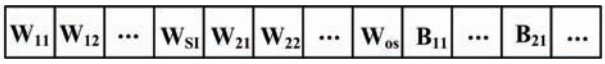

Fig. 4 *Structure of the chromosome.*

Crossover: The crossover probability P_c controls the rate at which solutions are subjected to crossover. In this paper, P_c is defined as

$$P_{\mathrm{c}} = \begin{cases} k_1 \left(f_{\max} - f'\right) / \left(f_{\max} - \bar{f}\right), f' \geq \bar{f} \\ k_3, \qquad\qquad\qquad\qquad f' < \bar{f} \end{cases}, \tag{3}$$

Mutation: The mutation probability P_m controls the speed of GAs in exploring a new area. In this paper, P_m is defined as

$$P_{\mathrm{m}} = \begin{cases} k_2 \left(f_{\max} - f\right) / \left(f_{\max} - \bar{f}\right), f \geq \bar{f} \\ k_4, \qquad\qquad\qquad\qquad f < \bar{f} \end{cases}, \tag{4}$$
$$0 \leq k_1, k_2, k_3, k_4 \leq 1.0$$

where $f_{\max}$ is the maximum fitness value of the population, $\bar{f}$ is the average fitness value of the population, f' is the larger of the fitness values of the solutions to be crossed, f denotes the fitness value of the population, and k_1, k_2, k_3, and k_4 are the constants of proportionality.

(5) After finishing genetic algorithms, the BP neural network is trained until the errors converge to the required precision.

The flowchart of BP neural network optimized by GA is shown in Fig. 5.

4. Engineering applications

According to the classification methods of slope structures [11], the left abutment slope can mainly be categorized in three types: consequent toppling block, wedge with two sliding surfaces and massive slope structure. Therefore, the geological condition of the dam abutment on the left bank at Jinping I is very complicated. In this study, several important parameters, including the slope geological conditions, location of instruments, space and time conditions before and after measuring, were used as the input parameters, while the slope displacement was the output parameter.

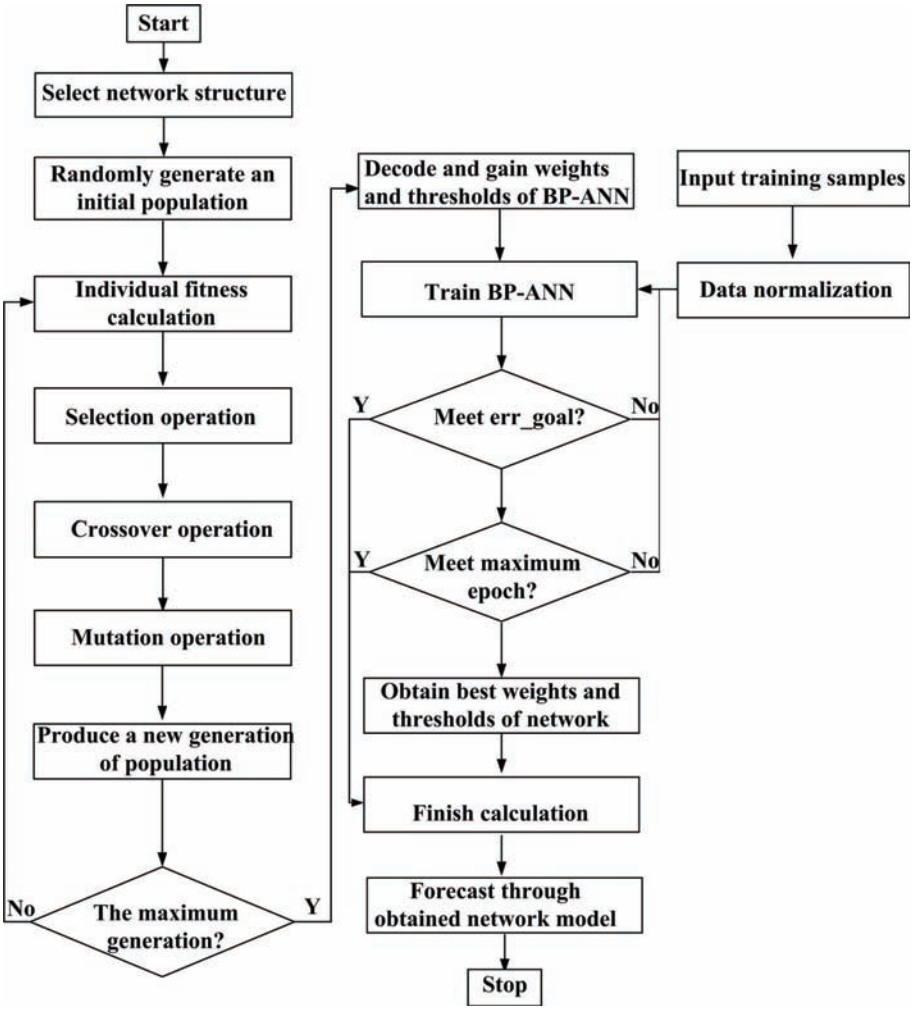

Fig. 5 *Flowchart of BP neural network optimized by GA.*

(1) Geological conditions: The modulus of elasticity X_1 and the classification of rock masses X_2 were adopted as geological parameters in this work.

(2) Location of instruments: In order to accurately represent the location of instruments, the installation height of instruments X_3 was introduced here to position those instruments. The monitoring instruments used in this project include 53 multipoint-displacement meters, 40 bolt stress meters, and 183 anchor load cells. Due to space limitations, the layout of monitoring instruments is not listed here.

(3) Space and time condition before start measuring: The excavation height of slope X_4 and the start time X_5 before measurement were used here.

(4) Space and time condition after measurement: The complete measuring time cycle X_6 was introduced here to express the time effect relationship between rock mass deformation and excavation of slope, and the actual excavation height after measurement X_7 was also introduced to express the whole excavation relationship between rock mass deformation and slope in this work.

In the proposed neural network model for prediction of slope stability, several important parameters, including the modulus of elasticity X_1, the classification of rock masses X_2, the installation height of instruments X_3, the excavation height of slope X_4, the start measuring time X_5, the complete measuring time cycle X_6 and the actual excavation height after measurement X_7 were used as the input parameters, while the slope displacement was the output parameter. 120 cases were selected as training samples, as shown in Tab. I. Based on the foregoing GA-BP hybrid algorithm procedure and the established mathematical model, the predictive model of hybrid algorithm was established in Matlab to train these samples. In the training process of the target samples, the sum-squared error was 1.0×10^{-10}, and the maximum numbers of training steps were 200. The GA parameters of the hybrid algorithm were: population size 120, generation number 10, crossover probability 0.1, and mutation probability 0.05.

No.	Instrument tag Number	X_1 (GPa)	X_2	X_3 (m)	X_4 (m)	X_5 (d)	X_6 (d)	X_7 (m)	Measured displacement u (mm)
1	M1	13	4	183.8	237.5	222	37	7.5	0.16
2	M1	13	4	183.8	237.5	222	107	22.5	0.51
3	M1	13	4	183.8	237.5	222	188	37.5	1.52
4	M1	13	4	183.8	237.5	222	212	52.5	2.16
5	M1	13	4	183.8	237.5	222	226	67.5	2.45
6	M1	13	4	183.8	237.5	222	286	82.5	3.62
7	M10	15	4	80	140	93	47	15	0.15
8	M10	15	4	80	140	93	96	45	0.35
9	M10	15	4	80	140	93	187	75	0.45
10	M10	15	4	80	140	93	292	90	0.54
11	M10	15	4	80	140	93	354	105	0.76
12	M10	15	4	80	140	93	417	120	1.01
13	M10	15	4	80	140	93	505	135	1.13
14	M10	15	4	80	140	93	543	165	1.24
15	M10	15	4	80	140	93	586	175	1.27
16	M10	15	4	80	140	93	592	180	1.29
17	M11	9	5	110	140	56	28	15	0.03
18	M11	9	5	110	140	56	77	45	0.05
19	M11	9	5	110	140	56	168	75	0.62
20	M11	9	5	110	140	56	273	90	1.92
21	M11	9	5	110	140	56	335	105	2.82
22	M11	9	5	110	140	56	398	120	4.13
23	M11	9	5	110	140	56	486	135	4.55
24	M11	9	5	110	140	56	510	150	4.6
25	M11	9	5	110	140	56	524	165	4.7

26	M11	9	5	110	140	56	573	180	4.81
27	M11C3L	15	4	301	335	125	6	15	0.53
28	M11C3L	15	4	301	335	125	55	35	0.6
29	M12	16	4	138	185	37	54	30	0.08
30	M12	16	4	138	185	37	159	45	−0.15
31	M12	16	4	138	185	37	284	75	0.06
32	M12	16	4	138	185	37	372	90	0.36
33	M12	16	4	138	185	37	396	105	0.41
34	M12	16	4	138	185	37	410	120	0.61
35	M12	16	4	138	185	37	453	130	1.49
36	M12	16	4	138	185	37	459	135	1.61
37	M2	15	4	213.8	245	168	70	15	0.75
38	M2	15	4	213.8	245	168	151	30	1.46
39	M2	15	4	213.8	245	168	175	45	1.56
40	M2	15	4	213.8	245	168	189	60	1.64
41	M2	15	4	213.8	245	168	232	70	1.78
42	M2C3L	10	5	275.5	290	16	19	15	4.45
43	M2C3L	10	5	275.5	290	16	62	25	5.66
44	M2C3L	10	5	275.5	290	16	145	60	6.74
45	M3	17	4	183.8	215	146	51	11	0.41
46	M3	17	4	183.8	219	146	113	26	0.55
47	M3	17	4	183.8	219	146	176	41	0.61
48	M3	17	4	183.8	219	146	264	56	0.66
49	M3	17	4	183.8	219	146	288	71	0.73
50	M3	17	4	183.8	219	146	302	86	0.79
51	M3	17	4	183.8	219	146	351	101	0.86
52	M3C3L	0	0	302	335	106	24	15	0.6
53	M3C3L	17	4	302	335	106	73	35	1.1
54	M4	11	4	213.8	237.5	153	15	7.5	0.14
55	M4	11	4	213.8	237.5	153	78	22.5	2.65
56	M4	11	4	213.8	237.5	153	166	37.5	3.6
57	M4	11	4	213.8	237.5	153	190	52.5	3.94
58	M4	11	4	213.8	237.5	153	204	67.5	4.06
59	M4	11	4	213.8	237.5	153	247	77.5	4.53
60	M4C3L	17	4	333.5	350	39	39	20	−0.01
61	M5	15	4	153.8	185	69	163	45	−1.68
62	M5	15	4	153.8	185	69	218	60	−1.51
63	M5	15	4	153.8	185	69	260	75	−1.32
64	M5	15	4	153.8	185	69	282	90	−0.93
65	M5	15	4	153.8	185	69	428	120	1.92
66	M5	15	4	153.8	185	69	471	130	2.33
67	M5	15	4	153.8	185	69	477	135	2.43
68	M6	16	4	185	250	285	16	25	−0.77
69	M6	16	4	185	250	285	127	40	−0.87
70	M6	16	4	185	250	285	162	55	−0.98
71	M6	16	4	185	250	285	205	65	−1
72	M6	16	4	185	250	285	211	70	−1.02
73	M6C3L	15	4	247	268	42	12	7	−0.05
74	M6C3L	15	4	247	268	42	123	22	−0.13

75	M6C3L	15	4	247	268	42	158	37	−0.23
76	M6C3L	15	4	247	268	42	201	47	−0.24
77	M6C3L	15	4	247	268	42	256	67	−0.3
78	M6C3L	15	4	247	268	42	333	102	−0.3
79	M7	9	5	213.8	238	133	14	7	0.41
80	M7	9	5	213.8	238	133	56	22	2.54
81	M7	9	5	213.8	238	133	189	52	5.29
82	M7	9	5	213.8	238	133	224	67	6.13
83	M7	9	5	213.8	238	133	267	77	7.4
84	M7	9	5	213.8	238	133	273	82	7.4
85	M7C3L	17	4	277	305	148	18	10	0.07
86	M7C3L	17	4	277	305	148	73	30	2.96
87	M7C3L	17	4	277	305	148	150	65	5.59
88	M8	17	4	17.32	51	100	75	29	−0.73
89	M8	17	4	17.32	51	100	131	59	−0.57
90	M8	17	4	17.32	51	100	156	89	−0.57
91	M8	17	4	17.32	51	100	215	104	−0.58
92	M8	17	4	17.32	51	100	264	134	−0.55
93	M8	17	4	17.32	51	100	355	164	−0.55
94	M8	17	4	17.32	51	100	460	179	−0.75
95	M8	17	4	17.32	51	100	522	194	−0.85
96	M8	17	4	17.32	51	100	585	209	−0.84
97	M8	17	4	17.32	51	100	673	224	−0.87
98	M8	17	4	17.32	51	100	697	239	−0.88
99	M8	17	4	17.32	51	100	711	254	−0.87
100	M8	17	4	17.32	51	100	754	264	−0.88
101	M9	17	4	45.53	69.5	70	31	10.5	−0.11
102	M9	17	4	45.53	69.5	70	87	40.5	0
103	M9	17	4	45.53	69.5	70	171	85.5	0.15
104	M9	17	4	45.53	69.5	70	220	115.5	0.2
105	M9	17	4	45.53	69.5	70	311	145.5	0.25
106	M9	17	4	45.53	69.5	70	416	160.5	0.27
107	M9	17	4	45.53	69.5	70	478	175.5	0.29
108	M9	17	4	45.53	69.5	70	541	190.5	0.31
109	M9	17	4	45.53	69.5	70	629	205.5	0.33
110	M9	17	4	45.53	69.5	70	653	220.5	0.35
111	M9	17	4	45.53	69.5	70	667	235.5	0.35
112	M9	17	4	45.53	69.5	70	710	245.5	0.38
113	M9	17	4	45.53	69.5	70	716	250.5	0.4
114	M9C3L	17	4	241.45	245	11	61	15	0.43
115	M9C3L	17	4	241.45	245	11	142	30	0.68
116	M9C3L	17	4	241.45	245	11	166	45	0.7
117	M9C3L	17	4	241.45	245	11	223	70	0.74
118	M9C3L	17	4	241.45	245	11	278	90	0.6
119	M9C3L	17	4	241.45	245	11	306	105	0.54
120	M9C3L	17	4	241.45	245	11	355	125	0.53

Tab. I *Training samples.*

The results of the GA-BP hybrid algorithm after running the program are shown in Figs. 6–8. From the results it can be clearly seen that, the hybrid algorithm model carries on 10 generations of genetic evolution operation to train and optimize

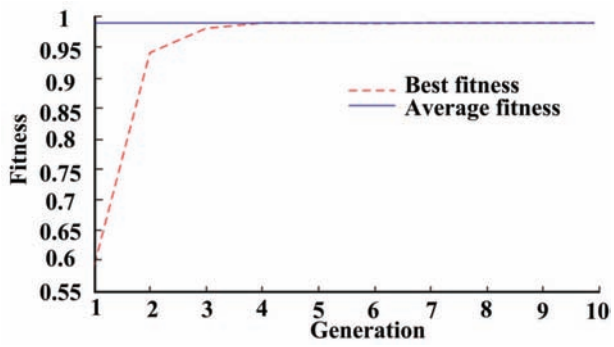

Fig. 6 *Fitness curves of GA.*

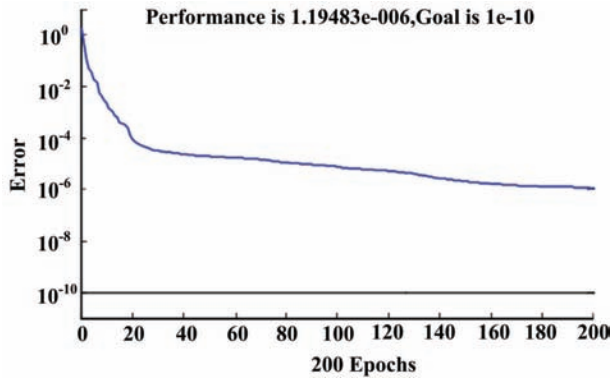

Fig. 7 *Training error curve of GA-BP hybrid algorithm.*

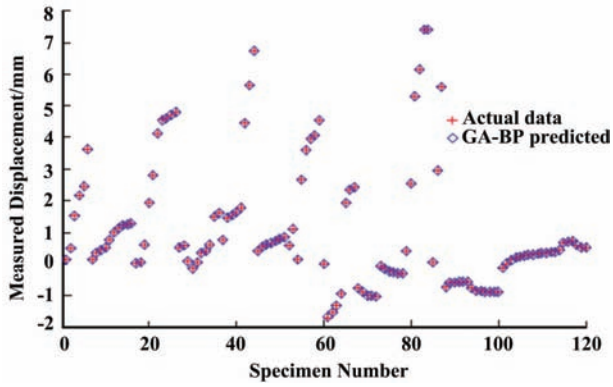

Fig. 8 *Comparison between the actual data and the predicted values.*

the network weights and thresholds, which obtains the best training results as the initial input values of the neural network model to be trained. Then, the network model was trained until getting the desired network error only by 200 steps (see Fig. 7).

In order to better compare the forecast accuracy of GA-BP algorithms, except for the 120 training samples, 15 samples were randomly selected as samples to test the model forecast accuracy, as shown in Tab. II. The comparison of the forecast results obtained by GA-BP algorithm and the actual data is shown in Fig. 9. It can be obviously seen that the forecasted results agree well with the actual data.

No.	Instrument Tag Number	X_1 (GPa)	X_2	X_3 (m)	X_4 (m)	X_5 (d)	X_6 (d)	X_7 (m)	Measured displacement u (mm)
1	M1	13	4	183.8	237.5	222	269	77.5	3.62
2	M10	15	4	80	140	93	529	150	1.23
3	M11	9	5	110	140	56	567	175	4.75
4	M12	16	4	138	185	37	221	60	−0.1
5	M2	15	4	213.8	245	168	249	75	1.78
6	M2C3L	10	5	275.5	290	16	117	45	6.21
7	M3	17	4	183.8	219	146	345	96	0.83
8	M4	11	4	213.8	237.5	153	253	82.5	4.53
9	M5	15	4	153.8	185	69	393	105	0.91
10	M6C3L	15	4	247	268	42	284	82	−0.3
11	M7	9	5	213.8	238	133	78	37	3.16
12	M7C3L	17	4	277	305	148	101	45	4.15
13	M8	17	4	17.32	51	100	760	269	−0.89
14	M9	17	4	45.53	69.5	70	112	70.5	0.1
15	M9C3L	17	4	241.45	245	11	180	60	0.74

Tab. II *Testing samples.*

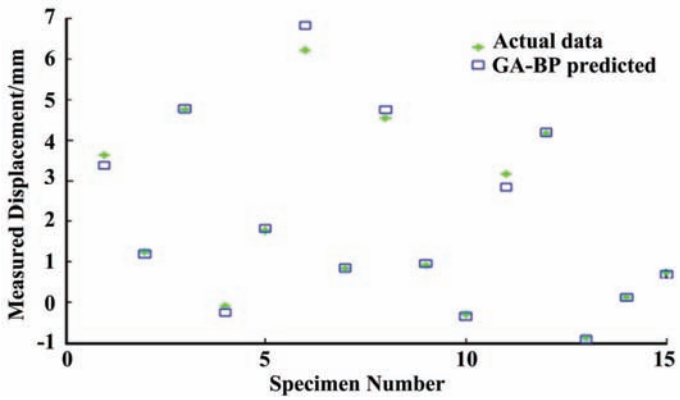

Fig. 9 *Comparison between the actual data and the predicted values.*

5. Conclusions

GA has been proved to be capable of finding global optima in complex problems by exploring virtually all regions of the state space and exploiting promising areas through mutation, crossover and selection operations applied to individuals in the populations. It applies selection, crossover and mutation operators to construct fitter solutions. In this study, a hybrid model based on the combination of GA and BP neural network is proposed to improve the forecasting performance. GA is employed to optimize the weight and threshold of the BP neural network. Then, the GA-BP model was successfully applied to the left abutment slope of Jinping I hydropower station, which provides a new method for predicting and analyzing slope stability of the similar projects. In this study, the GA-BP network model is trained until getting the desired network error only by 200 steps and the forecasted results agree well with the actual data. It is concluded that such GA-BP model is a reliable, simple and valid computational tool for accurate prediction of the slope stability.

References

[1] CHO S.E. Probabilistic stability analyses of slopes using the ANN-based response surface. *Comput Geotech*. 2009, 36(5), pp. 787-797, doi: 10.1016/j.compgeo.2009.01.003.

[2] DAWSON E.M., ROTH W.H., DRESCHER A. Slope stability analysis by strength reduction. *Geotechnique*. 1999, 49(6), pp. 835-840, doi: 10.1680/geot.1999.49.6.835.

[3] JIANG G.L., MAGNAN J.P. Stability analysis of embankments: Comparison of limit analysis with methods of slices. *Geotechnique*. 1997, 47(4), pp. 857-872, doi: 10.1680/geot.1997.47.4.857.

[4] JURGEN B. Neural networks for cost estimation: Simulations and pilot application. *Int J Prod Res*. 2000, 38(6), pp. 1231-1254, doi: 10.1080/002075400188825.

[5] KUMAR S., NARESH R. Efficient real coded genetic algorithm to solve the non-convex hydrothermal scheduling problem. *Int J Elec Power Energy Syst*. 2007, 29(10), pp. 738-747, doi: 10.1016/j.ijepes.2007.06.001.

[6] LIN Y., HE Z., LI B., YANG Q. Slope stability analysis based on a multigrid method using a nonlinear 3D finite element model. *Front. Struct. Civ. Eng.* 2013, 7(1), pp. 24-31, doi: 10.1007/s11709-013-0190-1.

[7] LIN H.M., CHANG S.-K., WU J.-H., JUANG C.H. Neural network-based model for assessing failure potential of highway slopes in the Alishan, Taiwan Area: Pre- and post-earthquake investigation. *Eng Geol*. 2009, 104(3-4), pp. 280-289, doi: 10.1016/j.enggeo.2008.11.007.

[8] SAKELLARIOU M.G., FERENTINOU M.D. A study of slope stability prediction using neural networks. *Geotech Geol Eng*. 2005, 23(4), pp. 419-445, doi: 10.1007/s10706-004-8680-5.

[9] SUN J.P., LI J.C., LIU Q.Q. Search for critical slip surface in slope stability analysis by spline-based GA method. *J Geotech Geoenviron Eng.* 2008, 134(2), pp. 252-256, doi: 10.1061/(ASCE)1090-0241(2008)134:2(252).

[10] SONG S.W., CAI D., FENG X., CHEN X., WANG D. Safety monitoring and stability analysis of left abutment slope of Jinping I hydropower station. *J Rock Mech Geotech Eng.* 2011, 3(2), pp. 17-130, doi: 10.3724/SP.J.1235.2011.00117.

[11] SONG S.W., YAN M. Stability evaluation based classification method for rock mass structures in rock slope. *J Eng Geol*. 2011, 19(1), pp. 6-11. In Chinese.

[12] WU S.Y., SHEN M.B., WANG J. Jinping hydropower project: main technical issues on engineering geology and rock mechanics. *Bull Eng Geol Environ*. 2010, 69(3), pp. 325-332, doi: 10.1007/s10064-010-0272-4.

[13] XU N.W., TANG C.A., LI L.C., ZHOU Z., SHA C., LIANG Z.Z., YANG J.Y. Microseismic monitoring and stability analysis of the left bank slope in Jinping first stage hydropower station in southwestern China. *Int J Rock Mech Min.* 2011, 48(6), pp. 950-963, doi: 10.1016/j.ijrmms.2011.06.009.